Microwave Engineering
Ulm University

ulm university universität
uulm

On the Impact of Hardware Impairments in Noncoherent Massive MIMO Systems

Stephan Bucher, George Yammine, Robert F.H. Fischer, Christian Waldschmidt

On the Impact of Hardware Impairments in Noncoherent Massive MIMO Systems

Stephan Bucher[1], George Yammine[2], Robert F.H. Fischer[2], and Christian Waldschmidt[1]
[1]Institute of Microwave Engineering, [2]Institute of Communications Engineering
Ulm University, 89081 Ulm, Germany
Email: {stephan.bucher, george.yammine, robert.fischer, christian.waldschmidt}@uni-ulm.de

***Abstract*—Massive MIMO systems, where a very large number of antennas are employed at the base station, are one of the key technologies to increase the capacity in multi-user MIMO scenarios. This comes at the price of raised hardware costs and power consumption, which scales linearly with the number of receiver chains. Hence, a low-cost and power-efficient hardware design is of special interest. However, such a low-complexity radio frontend impairs the quality of the received signal, impacting the overall system performance. In this paper, the robustness to hardware impairments at the base station is analyzed when noncoherent detection schemes are applied in the uplink transmission. The effects on the system performance are assessed by means of numerical simulations. Behavioral and stochastic impairment models are utilized to cover the influence of the main hardware components, i.e., amplifiers, local oscillators, and analog-to-digital converters. A cluster-based channel model adapted to the massive MIMO setting forms the basis for the evaluation. It is shown that highly-linear amplifiers are integral for optimum performance. However, low-resolution ADCs and oscillators of moderate quality can be employed without sacrificing performance, saving power and costs.**

I. Introduction

In order to satisfy the rising demand of high spectral efficiency in wireless communication systems, massive multiple-input/multiple-output (MIMO) systems have attracted growing attention over the last years [1], [2]. Here, a moderate number of users communicate with a central base station (BS) equipped with a large number of antennas aiming enhanced capacity. Generally, accurate channel state information (CSI) acquired by means of pilot signaling is required to take advantage of such systems. In order to overcome the challenging channel estimation process, noncoherent detection schemes have been proposed [3], [4], where the (known) spatial power distribution of each user at the BS is utilized instead of the actual channel estimates. The presented schemes are able to achieve results comparable to CSI-based detection [5]–[8].

Despite of the benefits of massive MIMO systems, the cost and power consumption scale linearly with the number of radio frequency (RF) chains at the BS. Hence, a circuit-aware design is of major interest, where high performance is achieved but power-efficient and low-cost hardware is employed at the same time. This paper explores the robustness of the proposed noncoherent detection to hardware imperfections/impairments at the BS caused by the main receiver components. This includes the non-linear distortions of the low-noise amplifier (LNA), the phase noise of the local oscillator (LO), and the quantization errors of the analog-to-digital converter (ADC). To this end, behavioral and stochastic impairment models are utilized to carry out the performance analysis. A cluster-based channel model is used to represent the propagation in a massive MIMO scenario in a physically accurate manner.

The paper is organized as follows. Besides a brief recapitulation of the uplink transmission model and the noncoherent detection in massive MIMO, the respective impairment models are introduced in Section II. Numerical results are presented in Section III and conclusions are drawn in Section IV.

This work was funded by the Deutsche Forschungsgemeinschaft (DFG, German Research Foundation) — WA 3506/5-1; FI 982/12-1.

II. System Model and Noncoherent Detection

A. Uplink Transmission Model

In this paper, a multi-user uplink scenario is considered as depicted in Fig. 1. N_{u} single-antenna users simultaneously transmit to a central BS equipped with $N_{\mathsf{rx}} \gg N_{\mathsf{u}}$ antennas, which corresponds to a massive MIMO setup. In the following, single-carrier transmission is assumed and all signals are modeled in the equivalent complex baseband. The symbols $b_{k,u}$ transmitted by user u at the discrete time step k are differentially encoded unit-magnitude phase-shift keying (DPSK) symbols and are given by

$$b_{k,u} = a_{k,u}\, b_{k-1,u}\,, \qquad b_{0,u} = 1\,, \tag{1}$$

where $a_{k,u}$ are the data symbols drawn from an M-ary PSK constellation $\mathcal{M} = \{\mathrm{e}^{\mathrm{j}2\pi i/M} \mid i = 0, 1, \ldots, M-1\}$. Assuming the propagation channel to remain constant over a transmission burst and omitting inter-symbol interference, the received signal at time instant k can be written as

$$\boldsymbol{r}_k = \underbrace{\sum_{u=1}^{N_{\mathsf{u}}} \boldsymbol{h}_u b_{k,u}}_{\boldsymbol{u}_k} + \boldsymbol{n}_k\,, \tag{2}$$

where $\boldsymbol{h}_u = [h_{1,u}, \ldots, h_{N_{\mathsf{rx}},u}]^{\mathsf{T}}$ collects the complex-valued channel coefficients from user u to the N_{rx} receive antennas and $\boldsymbol{n}_k = [n_{1,k}, \ldots, n_{N_{\mathsf{rx}},k}]^{\mathsf{T}}$ gathers the zero-mean circular-symmetric complex Gaussian noise samples with variance σ_{n}^2. The signal-to-noise ratio (SNR), which is defined as the ratio of the transmitted energy per PSK symbol $E_{\mathsf{s,tx}}$ and the noise power spectral density N_0, reads $E_{\mathsf{s,tx}}/N_0 = 1/\sigma_{\mathsf{n}}^2$.

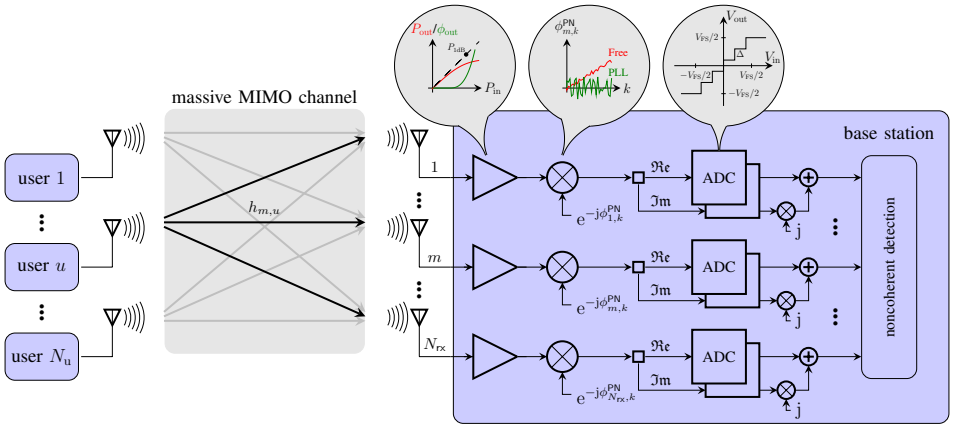

Fig. 1. Generic system model for the massive MIMO uplink transmission including the main hardware components at the base station.

Modeling the massive MIMO channel using a geometry-based stochastic approach, more specifically the COST 2100 channel model [9], [10], the channel coefficients $h_{m,u}$ between user u and BS antenna m can be expressed by [6]

$$h_{m,u} = \sum_i a_{i,m,u}^{\mathsf{MPC}} \, C_{\mathsf{rx}}(\varphi_{i,m,u}^{\mathsf{MPC}}, \theta_{i,m,u}^{\mathsf{MPC}}) \, , \tag{3}$$

where $a_{i,m,u}^{\mathsf{MPC}}$ is the complex amplitude of the ith multi-path component due to active clusters with the corresponding direction of arrivals (DOAs) $\varphi_{i,m,u}^{\mathsf{MPC}}$ and $\theta_{i,m,u}^{\mathsf{MPC}}$, respectively. The antenna pattern at the BS is taken into account by $C_{\mathsf{rx}}(\varphi, \theta)$.

B. Noncoherent Detection

At the BS, noncoherent detection schemes are applied. To this end, a receive block $\boldsymbol{R}$ over N_{bl} time steps is considered, which is given in case of an ideal receiver by

$$\boldsymbol{R} = [\boldsymbol{r}_0, \cdots, \boldsymbol{r}_{N_{\mathsf{bl}}-1}] \, . \tag{4}$$

Decision-feedback differential detection combined with noncoherent decision-feedback equalization (DFDD/nDFE) [4] of user u is then based on the $N_{\mathsf{bl}} \times N_{\mathsf{bl}}$ correlation matrix

$$\boldsymbol{Z}_u \stackrel{\text{def}}{=} \boldsymbol{R}^{\mathsf{H}} \boldsymbol{W}_u \boldsymbol{R} \, , \tag{5}$$

where $\boldsymbol{W}_u \stackrel{\text{def}}{=} \mathbf{diag}(w_{1,u}, \ldots, w_{N_{\mathrm{rx}},u})$ is a user-specific diagonal weighting matrix, which effectively acts as a spatial-domain filter. The weighting coefficients $w_{m,u}$ can be optimized to maximize the signal-to-noise-plus-interference ratio (SINR) [11], when the average receive power (power-space profile, PSP) of the individual user at the BS is known. Assuming an ideal receiver with no impairments, the PSP $\boldsymbol{p}_u$ of user u stems from the channel coefficient vector $\boldsymbol{h}_u$ and the transmitted user symbols $b_{k,u}$ during the transmission burst by averaging over different channel realizations and the transmit symbols as follows

$$\boldsymbol{p}_u \stackrel{\text{def}}{=} \mathrm{E}\{|\boldsymbol{h}_u b_{k,u}|^2\} \, . \tag{6}$$

C. Uplink with Hardware Impairments

At the BS, hardware imperfections cause different types of distortions onto the desired receive signal $\boldsymbol{r}_k$. In the following, accurate models for the main hardware impairments as depicted in Fig. 1 are introduced capturing the non-linear distortions of the LNAs, the phase noise of the LOs used for downconversion, and the course quantization effects after the analog-to-digital conversion. The impact on the received signal is analyzed separately for each component.

1) Non-Linear Amplifier: The non-linear behavior of the amplifiers are commonly modeled by Volterra series or its variants [12]–[15]. These computational complex models are able to capture the non-linear effects associated with wideband signals by means of memory structures. However, in case of narrowband systems, memoryless (polynomial) models [16] are sufficient to describe the instantaneous behavior in terms of amplitude-to-amplitude (AM-AM) and amplitude-to-phase (AM-PM) effects, whereby both the amplitude and the phase at the output are dependent on the instantaneous input signal amplitude (see Fig. 1). Assuming that the amplifier at each receiving branch follows the same input-output relation, the output signal $\hat{r}_{m,k}$ at the mth branch and at the time step k using a polynomial of order $2P+1$ is

$$\hat{r}_{m,k} = \sum_{p=0}^{P} G_{2p+1} |u_{m,k}|^{2p} u_{m,k} + n_{m,k} \, , \tag{7}$$

where G_{2p+1} are complex coefficients. Generally, fifth-order polynomials are sufficient to reflect the non-linear characteristics in an accurate manner. Even-order terms are neglected in (7) since they only lead to out-of-band spectral regrowth [16]. In order to keep the amplifiers at each receive branch in the linear operation region and to avoid distortions, the amplifiers have to be backed-off. The input back-off (IBO) is defined as the ratio of the input-related $1\,\mathrm{dB}$ compression point $P_{1\mathrm{dB,in}}$ of the amplifier and the maximum average input power $\overline{P}_{\mathrm{in,max}}$ among all amplifiers of the receive branches as follows

$$\mathrm{IBO} = 10 \log_{10} \left(\frac{P_{1\mathrm{dB,in}}}{\overline{P}_{\mathrm{in,max}}} \right) \mathrm{dB} \, . \tag{8}$$

2) Phase Noise: The received signal is impaired by the phase noise of the imperfect LO signal used for downconversion. Assuming perfect timing and frequency synchronization, the resultant received vector $\hat{\boldsymbol{r}}_k$ can be expressed by

$$\hat{\boldsymbol{r}}_k = \boldsymbol{D}_k \boldsymbol{u}_k + \boldsymbol{n}_k \,, \tag{9}$$

where

$$\boldsymbol{D}_k = \mathbf{diag}\left(\mathrm{e}^{-\mathrm{j}\phi^{\mathsf{PN}}_{1,k}}, \cdots, \mathrm{e}^{-\mathrm{j}\phi^{\mathsf{PN}}_{N_{\mathrm{rx}},k}}\right) \tag{10}$$

models the respective phase drifts $\phi^{\mathsf{PN}}_{m,k}$ originated from the phase noise at each receive branch m and for each time step k. Here, two LO configurations at the BS can be analyzed, namely a common LO deployment, where a central LO serves all BS branches, or an independent LO deployment, where each receive path is equipped with a different LO. In the first case, the phase rotations are identical, i.e., $\phi^{\mathsf{PN}}_{1,k} = \ldots = \phi^{\mathsf{PN}}_{N_{\mathrm{rx}},k}$, and in the latter case all $\phi^{\mathsf{PN}}_{m,k}$ are independent.

In the following, the phase noise model of two common oscillator types, more precisely, of a free-running oscillator and of a frequency synthesizer with phase-locked loop (PLL), are introduced. In case of a free-running oscillator, the phase rotations can be modeled by a Wiener or Brownian motion process [16]–[18]. The phase error accumulates over time with linearly increasing variance (random walk) according to

$$\phi^{\mathsf{PN,FREE}}_{m,k} = \phi^{\mathsf{PN,FREE}}_{m,k-1} + \xi^{\mathsf{FREE}}_{m,k} \,, \tag{11}$$

where $\xi^{\mathsf{FREE}}_{m,k} \sim \mathcal{N}\left(0, \sigma^2_\xi\right)$ is a real Gaussian random variable of zero mean and variance

$$\sigma^2_\xi = 4\pi^2 f_0^2 c_{\mathrm{free}} T_{\mathsf{s}} \,, \tag{12}$$

which is a function of the carrier frequency f_0, the symbol duration time T_{s}, and a constant c_{free} characterizing the quality of the oscillator. The single-sideband phase noise spectrum $\mathcal{L}(f_{\mathrm{offset}})$ (in dBc/Hz) of the free-running oscillator at a specific frequency offset f_{offset} with respect to the oscillator frequency f_0 is specified by the quality constant c_{free}, which is approximately given by [18]

$$c_{\mathrm{free}} \approx 10^{\mathcal{L}(f_{\mathrm{offset}})/10} \left(\frac{f_{\mathrm{offset}}}{f_0}\right)^2 . \tag{13}$$

The presented phase noise model of a free-running oscillator has been extensively used in the literature [19]–[22]. However, in practice, PLL-based frequency synthesizers are employed in radio communication systems. These synthesizers comprise a voltage-controlled oscillator (VCO) and a high-quality reference crystal, which operates at low frequencies. A feedback loop involving a phase detector and a low-pass (loop) filter controls the output of the VCO via the reference signal. The output phase of the PLL can be represented by the sum of two stochastic processes [17], [23], [24], namely a Wiener process $\phi^{\mathsf{PN,REF}}_{m,k}$ of the reference signal and a one-dimensional Ornstein-Uhlenbeck process $\beta_{m,k}$, as follows

$$\phi^{\mathsf{PN,PLL}}_{m,k} = \phi^{\mathsf{PN,REF}}_{m,k} + \beta_{m,k} \,, \tag{14}$$

where

$$\phi^{\mathsf{PN,REF}}_{m,k} = \phi^{\mathsf{PN,REF}}_{m,k-1} + \xi^{\mathsf{REF}}_{m,k} \tag{15}$$

is again a random walk process as in case of a free-running oscillator with $\xi^{\mathsf{REF}}_{m,k} \sim \mathcal{N}\left(0, 4\pi^2 f_0^2 c_{\mathrm{ref}} T_{\mathsf{s}}\right)$ and the corresponding quality constant c_{ref} of the reference signal. Transferring the continuous-time representation of the Ornstein-Uhlenbeck process presented in [23] into a discrete-time model, $\beta_{m,k}$ in (14) can be expressed as [24]

$$\beta_{m,k} = \beta_{m,k-1} + 2\pi f_{c,\mathrm{PLL}} T_s / k_{\mathrm{PD}} \gamma_{m,k-1} + \xi^{\mathsf{VCO}}_{m,k} - \xi^{\mathsf{REF}}_{m,k} \,, \tag{16}$$

where $f_{c,\mathrm{PLL}}$ denotes the cut-off frequency of the PLL, k_{PD} is the phase detector constant, and $\xi^{\mathsf{VCO}}_{m,k}$ is a Gaussian distributed random variable according to $\xi^{\mathsf{VCO}}_{m,k} \sim \mathcal{N}\left(0, 4\pi^2 f_0^2 c_{\mathrm{vco}} T_{\mathsf{s}}\right)$ with the corresponding quality factor c_{vco} of the VCO. The VCO input is denoted by γ, which depends on the actual PLL design. Employing a charge pump PLL solving the steady state error, the VCO input phase is given by

$$\begin{aligned}\gamma_{m,k} = {} & \left(1 - 2\pi f_{c,\mathrm{PLL}} T_s\right) \gamma_{m,k-1} - 2\pi f_{c,\mathrm{CP}} T_s k_{\mathrm{PD}} \beta_{m,k-1} \\ & - k_{\mathrm{PD}} \left(\xi^{\mathsf{VCO}}_{m,k} + \xi^{\mathsf{REF}}_{m,k}\right) \,,\end{aligned} \tag{17}$$

where $f_{c,\mathrm{CP}}$ is the cut-off frequency of the charge pump. The respective VCO input for different PLL configurations, for instance with or without a first-order loop filter, can be found in [23], [24]. In general, the phase error grows without bound in case of a free-running oscillator, whereas the output phase of a PLL-based synthesizer is within a certain range, i.e., has bounded variance (see Fig. 1).

3) Analog-to-Digital Converter: The ADC quantizes the received signal to a resolution of q bits. Assuming that quantization is performed separately for the real and the imaginary component, the resultant receive signal after quantization can be expressed as

$$\hat{r}_{m,k} = \mathrm{Q}\{\mathfrak{Re}\{r_{m,k}\}\} + \mathrm{j}\mathrm{Q}\{\mathfrak{Im}\{r_{m,k}\}\} \,, \tag{18}$$

where $\mathrm{Q}\{\cdot\}$ denotes the nonlinear quantization function. Considering a uniform q-bit quantizer with a total input range V_{FS} and a quantization step-size $\Delta = V_{\mathrm{FS}}/(2^q - 1)$ as in Fig. 1, the quantized output of an input signal x can be given by

$$\mathrm{Q}\{x\} = \begin{cases} V_{\mathrm{FS}}/2, & x \geq V_{\mathrm{FS}}/2 \\ \left\lfloor \frac{x}{\Delta} \right\rceil \Delta, & -V_{\mathrm{FS}}/2 \leq x < V_{\mathrm{FS}}/2 \\ -V_{\mathrm{FS}}/2, & x < -V_{\mathrm{FS}}/2 \end{cases} , \tag{19}$$

where $\lfloor \cdot \rceil$ denotes rounding to the nearest smaller integer. In order to ensure a full-scale operation of the ADC and to avoid clipping, the input signal has to be amplified appropriately. Generally, a variable gain amplifier (VGA) and an automatic gain control (AGC) is employed. Analogously, the input range of the ADC has to be twice the maximum magnitude of the input signal according to

$$V_{\mathrm{FS}} = 2 \max\left\{|x|\right\} . \tag{20}$$

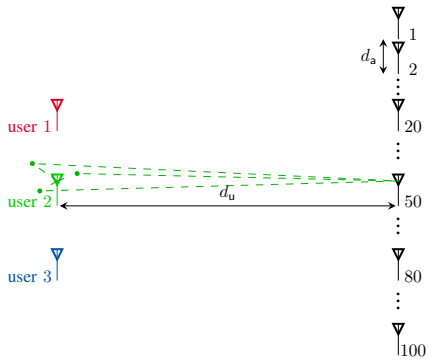

Fig. 2. User and BS arrangement. Multi-path propagation exemplarily depicted from user 2 to the 50th BS antenna.

III. Numerical Results

Numerical results were conducted for a three-user scenario ($N_\mathsf{u}=3$), where each user is located in the near-field of a physically-large BS consisting of $N_\mathsf{rx}=100$ antennas arranged as uniform linear array with an inter-element distance of $d_\mathsf{a}=\lambda$ (see Fig. 2). In the near-field scenario, the noncoherent detection scheme is highly dependent on the actual user position [6]. The users are arranged along a straight line parallel to the BS at a distance of $d_\mathsf{u}=10\,d_\mathsf{a}$ and are in front of the 20th, 50th, and 80th BS antenna, respectively.

A multi-path propagation channel is considered, where randomly placed clusters surround the users (local cluster) and the total number of multi-path components per user is three. The users are equipped with omni-directional antennas, whereas patch antennas are employed at the BS pointing into the direction of the users as in [7]. A power control is used assuming that the total receive power per user is one. To this end, the acquired channel matrices from the cluster-based channel model are normalized such that $||\boldsymbol{h}_u||^2=1$.

Regarding the noncoherent detection scheme, a transmission burst of $N_\mathsf{bl}=201$ symbols is considered, where each user transmits quaternary DPSK symbols. The performance measure is the symbol error rate (SER), which is averaged over 100,000 different channel realizations. In order to provide a comparison to coherent detection schemes, Bell Laboratories layered space-time (BLAST) [25] is evaluated as well for the presented scenario. Here, the channel coefficients are first estimated via pilot signals using Hadamard sequences of length 32 and a linear least-squares (LS) approach. Coherent detection is then applied on a transmission block of $N_\mathsf{bl}-32$ symbols. The associated rate loss compared to noncoherent detection is not considered nor compensated by means of higher-order modulation leading to a bias in favor of coherent detection. The parameters of the system configuration, the propagation channel and the (non)coherent detection scheme are summarized in Table I.

A. Non-Linear Amplifier

First, the impact of the non-linear amplifier on the SER performance is analyzed. To this end, a fifth-order polynomial without even-order terms is chosen to cover the non-linear characteristics of the amplifier. The corresponding complex coefficients G_{2p+1} in (7) are taken from [26] and are normalized to unity gain, hence $G_1=0.9989$, $G_3=0.0479\,\mathrm{e}^{-\mathrm{j}2.816}$, and $G_5=0.001\,\mathrm{e}^{\mathrm{j}0.39}$. The SER as function of the IBO for $E_{\mathsf{s,tx}}/N_0 \mathrel{\widehat{=}} 14\,\mathrm{dB}$ and for each user is depicted in Fig. 3. Generally, coherent and noncoherent detection perform almost identically for all users (plots overlap). The only exception is user 2, which performs slightly worse than the remaining users regarding noncoherent detection due to a higher overlap of the PSPs. As long as the amplifier is driven at large IBO, no impact on the SER performance is observed. However, approaching the non-linear operation region, the performance degrades. The degradation is moderate for $\mathrm{IBO}>0\,\mathrm{dB}$, which can be explained to some extent by the robustness of the differential phase modulation to amplitude and phase distortions. Strong degradation occur in the deep non-linear region.

Consequently, highly-linear (costly) amplifiers are still necessary for optimum performance. Otherwise an operation at moderate IBO has to be ensured to keep the performance degradation in an acceptable range corresponding to a loss in power efficiency.

TABLE I
System configuration and parameterization of propagation channel and (non)coherent detection.

System configuration	
number of users N_u	3
number of BS antennas N_rx	100
BS antenna spacing d_a	λ
user distance d_u	$10\,d_\mathsf{a}$
user antenna type	omni-directional
BS antenna type	patch [7]
Propagation channel	
cluster types	local
number of multi-path components per user	3
number of different channel realizations	100,000
channel normalization	$\|\|\boldsymbol{h}_u\|\|^2=1$
(Non)coherent detection	
modulation alphabet	4-ary DPSK
block length N_bl	201
pilot signal (length)	Hadamard (32)

B. Phase Noise

Next, the performance is assessed when the receive signal is distorted by phase noise induced by the local oscillator at downconversion to baseband. Here, a free-running oscillator and a PLL-based synthesizer in both common and independent LO deployment are considered. The SER is evaluated as function of the single-sideband phase noise density $\mathcal{L}(f_\mathrm{offset}=100\,\mathrm{kHz})$ in dBc/Hz at an offset frequency of 100 kHz, which directly specifies the quality of the LO in use and which is linked to the quality constants c_free and c_vco in the presented phase noise models, respectively. The symbol duration time is assumed to be $T_\mathsf{s}=100\,\mathrm{ns}$ [19] and the SNR is set to $E_{\mathsf{s,tx}}/N_0 \mathrel{\widehat{=}} 14\,\mathrm{dB}$.

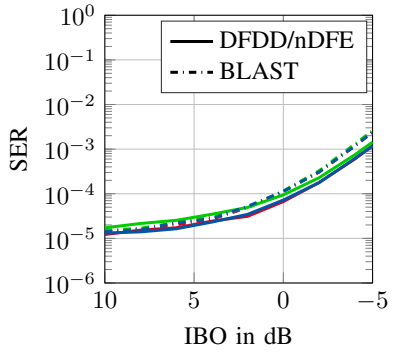

Fig. 3. Symbol error rate vs. IBO of a non-linear amplifier based on a fifth-order polynomial as in [26] for $E_{\mathsf{s,tx}}/N_0 \mathrel{\widehat{=}} 14\,\mathrm{dB}$. Colors correspond to users: user 1 (——), user 2 (——), user 3 (——).

Results using a free-running oscillator are depicted in Fig. 4a. Employing high- to medium-quality oscillators, the difference in the phase noise between successive samples is negligibly small. Consequently, the SER performance is not affected due to the differential encoding of the information symbols. However, the worse the quality of the oscillator the larger the phase deviations between consecutive samples, which deteriorates the SER when $\mathcal{L}(f_{\mathrm{offset}} = 100\,\mathrm{kHz}) > -90$ dBc/Hz. A performance improvement can be observed using a independent LO deployment due to an averaging of the independent phase noise sources. Regarding coherent detection, this effect was already observed in [20], [22]. Noteworthy, the coherent approach is more sensitive to phase noise distortions in both common and independent LO deployment.

Fig. 4b shows the SER performance for a PLL-based synthesizer employing a charge pump with $f_{c,\mathrm{CP}} = 16\,\mathrm{kHz}$. The cut-off frequency of the PLL is $f_{c,\mathrm{PLL}} = 50\,\mathrm{kHz}$ and the phase detector gain amounts to $k_{\mathrm{PD}} = 1$. The quality constant of the reference signal is chosen to be $c_{\mathrm{ref}} = 10^{-18}\,\mathrm{s}$. In comparison to a free-running oscillator, the phase noise is bounded and the phase shifts are smaller leading to a reduced phase noise sensitivity for both common and independent LO deployment. Furthermore, the performance gap between coherent and noncoherent detection is diminished.

Thus, due to the differential phase modulation, the performance degradation considering phase noise is less severe. Generally, medium-quality oscillators can be employed achieving optimum system performance. Due to an averaging effect of the phase noise sources, the quality of the oscillators can be lowered in independent LO deployments.

C. Analog-to-Digital Converter

Finally, the quantization effects due to the analog-to-digital conversion are taken into consideration. To this end, all ADCs are ensured to operate at full dynamic range and employ the same total input range. The SER as function of the resolution (in bits) at an SNR of $E_{\mathsf{s,tx}}/N_0 \mathrel{\widehat{=}} 14\,\mathrm{dB}$ is depicted in Fig. 5b. It can be observed that coarse quantization leads to a significant performance loss. In particular, the non-linear distortions of 1-bit quantizers result in a strong

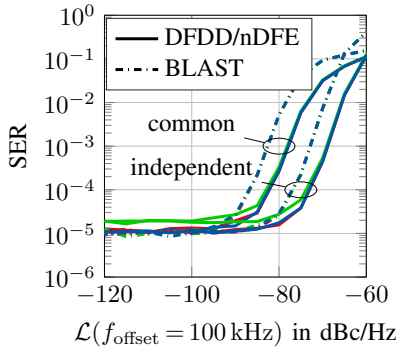

(a) Free-running oscillator.

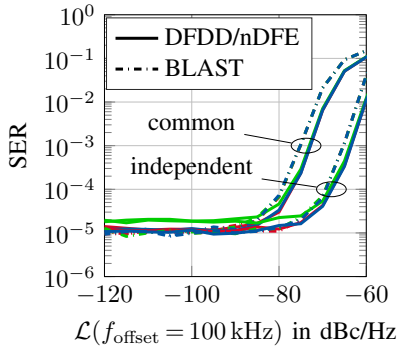

(b) PLL-based synthesizer.

Fig. 4. Symbol error rate vs. single-sideband phase noise density $\mathcal{L}$ in dBc/Hz at an offset frequency $f_{\mathrm{offset}} = 100\,\mathrm{kHz}$ for $E_{\mathsf{s,tx}}/N_0 \mathrel{\widehat{=}} 14\,\mathrm{dB}$. Colors correspond to users: user 1 (——), user 2 (——), user 3 (——).

degradation using channel-estimation-based detection. For the noncoherent case, the effective PSPs are estimated according to $\hat{\boldsymbol{p}}_u = \mathrm{E}\{|\mathrm{Q}\{\mathfrak{Re}\{\boldsymbol{h}_u b_{k,u}\}\} + \mathrm{j}\mathrm{Q}\{\mathfrak{Im}\{\boldsymbol{h}_u b_{k,u}\}|^2\}$. For 1-bit quantizers the resultant estimate turns into a uniform power distribution over the receive antennas for each user (see Fig. 5a). Consequently, no distinct PSPs are available at the BS to separate the users and detection fails. Interestingly, applying the original (ideal) PSPs instead, a significant performance gain is achieved even outperforming the coherent detection scheme (see Fig. 5b). However, the ideal PSPs cannot be acquired without an additional receive-power-estimation device in case of 1-bit quantization. Noteworthy, 4-bit ADCs still perform close to optimum. Hence, lower resolution ADCs can be employed without sacrificing performance. Since the power consumption of the ADC is related to the number of bits [27], the power efficiency can be enhanced substantially.

IV. Conclusion

In this paper, the impact of the hardware impairments at the BS has been investigated for a massive MIMO system, where noncoherent detection is applied in the uplink. The effects of the main receiver components were assessed on the basis of appropriate impairment models and a cluster-based channel model. It is shown that high-linearity amplifiers are still required to achieve the optimum performance. Alternatively, the input has to be backed-off, which in turn is inefficient in

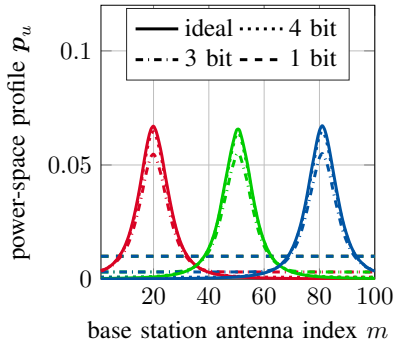

(a) Normalized effective power-space profile $\hat{\boldsymbol{p}}_u$ at different resolution of the ADCs.

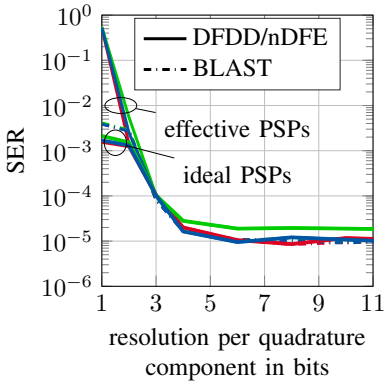

(b) Symbol error rate vs. resolution of the ADCs for $E_{\mathrm{s,tx}}/N_0 \mathrel{\widehat{=}} 14\,\mathrm{dB}$.

Fig. 5. System performance considering analog-to-digital conversion. Colors correspond to users: user 1 (——), user 2 (——), user 3 (——).

terms of power consumption. Due to the differential encoding of the transmit symbols, the phase noise sensitivity is small and therefore allows for oscillators of lower quality saving the overall costs. Coarse quantization leads to a significant performance loss, in particular for 1-bit resolution. Here, the users cannot be separated at the BS anymore due to uniform power-space profiles. A remarkable performance enhancement is achieved by applying the original (ideal) power-space profiles instead. However, the acquisition of the original profiles requires an additional receive-power-estimation circuitry when pure 1-bit quantization is performed. Generally, the resolution can be lowered to a few bits without loss in performance, which provides power-saving on a significant scale. A mixed-ADC architecture [28], where the base station is partially equipped with low- and high-resolution ADCs, can offer further potential in terms of power consumption and receive-power estimation remaining as open topic for future work.

References

[1] S. Yang *et al.*, "Fifty Years of MIMO Detection: The Road to Large-Scale MIMOs," *IEEE Communications Surveys & Tutorials*, vol. 17, no. 4, pp. 1941–1988, 2015.

[2] F. Rusek *et al.*, "Scaling Up MIMO: Opportunities and Challenges with Very Large Arrays," *IEEE Signal Processing Magazine*, vol. 30, no. 1, pp. 40–60, Jan. 2013.

[3] A. Schenk *et al.*, "Noncoherent Detection in Massive MIMO Systems," in *17th International ITG Workshop on Smart Antennas (WSA)*, Mar. 2013, pp. 1–8.

[4] R. F.H. Fischer *et al.*, "Noncoherent Decision-Feedback Equalization in Massive MIMO Systems," in *International Zurich Seminar on Communications (IZS)*, Feb. 2014, pp. 112–115.

[5] R. F.H. Fischer *et al.*, "Noncoherent Joint Decision-Feedback Detection in Multi-User Massive MIMO Systems," in *18th International ITG Workshop on Smart Antennas (WSA)*, March 2014, pp. 1–8.

[6] S. Bucher *et al.*, "Influence of Channel Parameters on Noncoherent Massive MIMO Systems," in *22nd International ITG Workshop on Smart Antennas (WSA)*, Mar. 2018.

[7] S. Bucher *et al.*, "Antenna Design for Noncoherent Massive MIMO Systems," in *15th International Symposium on Wireless Communication Systems (ISWCS)*, Aug. 2018.

[8] S. Bucher *et al.*, "A Noncoherent Massive MIMO System Employing Beamspace Techniques," *IEEE Transactions on Vehicular Technology*, pp. 1–1, 2019.

[9] L. Liu *et al.*, "The COST 2100 MIMO Channel Model," *IEEE Wireless Communications*, vol. 19, no. 6, pp. 92–99, Dec. 2012.

[10] R. Verdone *et al.*, Eds., *Pervasive Mobile and Ambient Wireless Communications*. Springer London, 2012.

[11] G. Yammine *et al.*, "On the Influence of the Antenna Pattern in Noncoherent Massive MIMO Systems," in *International Symposium on Wireless Communication Systems (ISWCS)*, Aug. 2015, pp. 391–395.

[12] M. Schetzen, *The Volterra and Wiener Theory of Nonlinear Systems*. Krieger Publishing Company, 2006.

[13] D. R. Morgan *et al.*, "A Generalized Memory Polynomial Model for Digital Predistortion of RF Power Amplifiers," *IEEE Transactions on Signal Processing*, vol. 54, no. 10, pp. 3852–3860, Oct. 2006.

[14] Hyunchul Ku *et al.*, "Behavioral Modeling of Nonlinear RF Power Amplifiers Considering Memory Effects," *IEEE Transactions on Microwave Theory and Techniques*, vol. 51, no. 12, pp. 2495–2504, Dec. 2003.

[15] L. Ding *et al.*, "A Robust Digital Baseband Predistorter Constructed Using Memory Polynomials," *IEEE Transactions on Communications*, vol. 52, no. 1, pp. 159–165, Jan. 2004.

[16] T. Schenk, *RF Imperfections in High-rate Wireless Systems*. Springer Netherlands, 2008.

[17] D. Petrovic *et al.*, "Effects of Phase Noise on OFDM Systems with and without PLL: Characterization and Compensation," *IEEE Transactions on Communications*, vol. 55, no. 8, pp. 1607–1616, Aug. 2007.

[18] A. Demir *et al.*, "Phase Noise in Oscillators: A Unifying Theory and Numerical Methods for Characterization," *IEEE Transactions on Circuits and Systems I: Fundamental Theory and Applications*, vol. 47, no. 5, pp. 655–674, May 2000.

[19] A. Pitarokoilis *et al.*, "Uplink Performance of Time-Reversal MRC in Massive MIMO Systems Subject to Phase Noise," *IEEE Transactions on Wireless Communications*, vol. 14, no. 2, pp. 711–723, Feb. 2015.

[20] E. Björnson *et al.*, "Massive MIMO with Non-Ideal Arbitrary Arrays: Hardware Scaling Laws and Circuit-Aware Design," *IEEE Transactions on Wireless Communications*, vol. 14, no. 8, pp. 4353–4368, Aug. 2015.

[21] E. Björnson *et al.*, "Distributed Massive MIMO in Cellular Networks: Impact of Imperfect Hardware and Number of Oscillators," in *23rd European Signal Processing Conference (EUSIPCO)*, Aug. 2015.

[22] A. Pitarokoilis *et al.*, "Performance of the Massive MIMO Uplink with OFDM and Phase Noise," *IEEE Communications Letters*, vol. 20, no. 8, pp. 1595–1598, Aug. 2016.

[23] A. Mehrotra, "Noise Analysis of Phase-Locked Loops," *IEEE Transactions on Circuits and Systems I: Fundamental Theory and Applications*, vol. 49, no. 9, pp. 1309–1316, Sep. 2002.

[24] S. Bittner *et al.*, "Tutorial on Discrete Time Phase Noise Modeling for Phase Locked Loops," 2008.

[25] G. J. Foschini *et al.*, "Analysis and Performance of Some Basic Space-Time Architectures," *IEEE Journal on Selected Areas in Communications*, vol. 21, no. 3, pp. 303–320, Apr. 2003.

[26] M. Faulkner *et al.*, "Spectral Sensitivity of Power Amplifiers to Quadrature Modulator Misalignment," *IEEE Transactions on Vehicular Technology*, vol. 41, no. 4, pp. 516–525, 1992.

[27] R. H. Walden, "Analog-to-Digital Converter Survey and Analysis," *IEEE Journal on Selected Areas in Communications*, vol. 17, no. 4, pp. 539–550, Apr. 1999.

[28] N. Liang *et al.*, "Mixed-ADC Massive MIMO," *IEEE Journal on Selected Areas in Communications*, vol. 34, no. 4, pp. 983–997, Apr. 2016.